J|A|C|S ARTICLES

Published on Web 09/01/2009

Mechanism of Hg−C Protonolysis in the Organomercurial Lyase MerB

Jerry M. Parks,*,† Hong Guo,†,‡ Cory Momany,§ Liyuan Liang,|| Susan M. Miller,⊥ Anne O. Summers,¶ and Jeremy C. Smith†,‡

UT/ORNL Center for Molecular Biophysics, Oak Ridge National Laboratory, 1 Bethel Valley Road, Oak Ridge, Tennessee 37831-6309, Department of Biochemistry and Cellular and Molecular Biology, University of Tennessee, Knoxville, Tennessee 37996, Department of Pharmaceutical and Biomedical Sciences, University of Georgia, Athens, Georgia 30602-7271, Environmental Science Division, Oak Ridge National Laboratory, Oak Ridge, Tennessee 37831, Department of Pharmaceutical Chemistry, University of California San Francisco, 600 16th Street, San Francisco, California 94158-2517, and Department of Microbiology, University of Georgia, Athens, Georgia 30602-2605

Received March 2, 2009; E-mail: parksjm@ornl.gov

Abstract: Demethylation is a key reaction in global mercury cycling. The bacterial organomercurial lyase, MerB, catalyzes the demethylation of a wide range of organomercurials via Hg−C protonolysis. Two strictly conserved cysteine residues in the active site are required for catalysis, but the source of the catalytic proton and the detailed reaction mechanism have not been determined. Here, the two major proposed reaction mechanisms of MerB are investigated and compared using hybrid density functional theory calculations. A model of the active site was constructed from an X-ray crystal structure of the Hg(II)-bound MerB product complex. Stationary point structures and energies characterized for the Hg−C protonolysis of methylmercury rule out the direct protonation mechanism in which a cysteine residue delivers the catalytic proton directly to the organic leaving group. Instead, the calculations support a two-step mechanism in which Cys96 or Cys159 first donates a proton to Asp99, enabling coordination of two thiolates with R−Hg(II). At the rate-limiting transition state, Asp99 protonates the nascent carbanion in a trigonal planar, bis thiol-ligated R−Hg(II) species to cleave the Hg−C bond and release the hydrocarbon product. Reactions with two other substrates, vinylmercury and *cis*-2-butenyl-2-mercury, were also modeled, and the computed activation barriers for all three organomercurial substrates reproduce the trend in the experimentally observed enzymatic reaction rates. Analysis of atomic charges in the rate-limiting transition state structure using Natural Population Analysis shows that MerB lowers the activation free energy in the Hg−C protonolysis reaction by redistributing electron density into the leaving group and away from the catalytic proton.

Introduction

Mercury is a highly mobile and reactive toxic element that is increasingly disseminated in the biosphere by human activities. Its elemental form, Hg(0), is susceptible to oxidation to Hg(II) via both biotic and abiotic processes.[1] Organomercuric species such as methylmercury,[2] $[CH_3Hg(II)]^+$, bioaccumulate and are highly toxic to living organisms, so understanding mechanisms of demethylation is of great interest.[3−5]

Scheme 1. Reaction Catalyzed by MerB (R = alkyl, aryl)

$$[R-Hg(II)]^+ \xrightarrow{\text{MerB}} [Hg(II)]^{2+} + R-H$$

Bacteria that carry the mercury resistance locus can degrade organomercurials by first cleaving the Hg−C bond to form Hg(II) and a hydrocarbon and then reducing Hg(II) to elemental Hg(0). The initial protonolysis reaction (Scheme 1) is catalyzed by the enzyme organomercurial lyase, MerB, for a wide variety of organomercurials with a rate acceleration of up to 10^7 relative to spontaneous abiotic decay.[6,7]

A fundamental question concerns the mechanism with which MerB achieves its catalytic effect. Early work on the MerB

† UT/ORNL Center for Molecular Biophysics, Oak Ridge National Laboratory.
‡ University of Tennessee, Department of Biochemistry and Cellular and Molecular Biology.
§ Department of Pharmaceutical and Biomedical Sciences, University of Georgia.
|| Environmental Science Division, Oak Ridge National Laboratory.
⊥ University of California San Francisco, Department of Pharmaceutical Chemistry.
¶ Department of Microbiology, University of Georgia.

(1) Barkay, T.; Miller, S. M.; Summers, A. O. *FEMS Microbiol. Rev.* **2003**, *27*, 355–384.
(2) Methylmercury is sometimes written as $CH_3Hg(I)$ in the mercury literature to convey the presence of only one site for binding of exchangeable ligands. Here, we adopt the conventional use of Roman numerals in parentheses to indicate the oxidation state of the metal ion, and a +1 charge outside the brackets to indicate the charge of the whole species: $[CH_3Hg(II)]^+$.
(3) Melnick, J. G.; Parkin, G. *Science* **2007**, *317*, 225–226.
(4) Omichinski, J. G. *Science* **2007**, *317*, 205–206.
(5) Strasdeit, H. *Angew. Chem., Int. Ed.* **2008**, *47*, 828–830.
(6) Begley, T.; Walts, A.; Walsh, C. *Biochemistry* **1986**, *25*, 7186–7192.
(7) Begley, T.; Walts, A.; Walsh, C. *Biochemistry* **1986**, *25*, 7192–7200.

10.1021/ja9016123 CCC: $40.75

mechanism showed that it functions as a monomer, contains four cysteine (Cys) residues,[6,7] lacks bound cofactors, and requires a 2-fold excess of free thiol such as cysteine or 2-mercaptoethanol for complete turnover in vitro. The pH-rate profile for MerB protonolysis of ethylmercuric chloride increased marginally up to pH 10.2, at which point the enzyme denatured. Significant solvent kinetic isotope effects suggested a kinetically important proton transfer in the rate-limiting step of the reaction, and there was no evidence for radicals or high-spin states. On the basis of their results, Begley et al. proposed an S_E2 mechanism in which three nucleophilic groups coordinate to R−Hg(II) and one of these provides the essential proton for Hg−C cleavage.[7]

Later work probed the reaction of *p*-hydroxymercuribenzoate (PHMB) with wild-type (WT) and mutant MerB enzymes and showed that Cys96 and Cys159 are each essential for activity. Cys160 is not required for catalysis, as evidenced by the retention of 37% WT activity for the Cys160Ser mutant,[8] but is important in removal of the Hg(II) product after protonolysis (S. Miller, unpublished data). Cys117 appears to play a structural, rather than catalytic, role. In the Cys159Ser mutant, the other three cysteine residues reacted more extensively with PHMB than in the WT, suggesting that Cys159 may be more reactive toward organomercurials in the WT and may form the initial enzyme−substrate covalent adduct. Pitts and Summers also found that the immediate source of the proton was a protein residue rather than the solvent and that the 2-fold excess of thiols was required for release of the product Hg(II) to complete the catalytic cycle.[8] These observations led to the proposal of a revised S_E2 mechanism in which the organomercurial Hg coordinates first with Cys159, followed by coordination to Cys96 with concomitant transfer of its proton directly to the leaving group.[8]

Recently, structures of free and Hg(II)-product-bound MerB have been solved by X-ray crystallography.[9,10] The active site structure of Hg(II)-product-bound MerB revealed trigonal coordination of Hg(II) by Cys96, Cys159, and a water molecule, consistent with model compound studies showing that two or more protein sulfur ligands are required to activate Hg−C bonds for protonolysis.[3−5,11−14]

Interestingly, the X-ray structures of Hg(II)-product-bound MerB also reveal weak coordination of Hg(II) by an aspartic acid carboxylate (Asp99), as evidenced by the Hg−O distance of ∼3 Å. Based on the Asp99Ala mutant, this residue has been found to be essential for activity (S. Miller, unpublished data). Although hydroxyl-[12] and ammonium-bearing[13] side chains have been suggested as potential proton donors in MerB catalysis, until the crystal structures appeared carboxyl-bearing side chains had not been proposed in the literature. On the basis of previous mechanistic hypotheses and their X-ray structures, Lafrance-Vanasse et al.[9] proposed that deprotonation of Cys96 by Asp99 enables attack of Cys96 on the organomercurial, and the subsequent or concurrent attack by Cys159 forms a trigonal R−Hg(II) species. In this model, Asp99 also donates the proton to the Hg−C bond to yield the Hg(II)-product-bound complex observed crystallographically.

Early computational studies using ab initio and density functional theory (DFT) methods to model the cleavage of methylmercury complexes by haloacids[15,16] were consistent with an S_E2 mechanism and showed that decreasing the electronegativity of the R−Hg(II) ligands lowers the activation barrier. More recently, DFT modeling of the protonolysis of chloromethylmercury and dimethylmercury by thiol(ate) ligands with ammonium as a proton source[13] found that coordination of Hg with multiple thiolates increases the negative charge on the leaving group carbon and facilitates Hg−C protonolysis.

Mechanistic simulations of enzyme reactions are often performed using quantum mechanical/molecular mechanical (QM/MM) methods.[17−19] Although this approach provides a realistic representation of the enzyme and solvent environment, the large number of degrees of freedom commonly results in difficulties associated with multiple local minima and/or insufficient statistical sampling. However, in favorable cases the energetics of bond breaking and forming are of significantly greater magnitude than long-range electrostatic effects such that a local, QM-only model of the enzyme active site is often sufficient for mechanistic studies of enzyme reactions.[20,21] Quantum chemical enzyme models have been used successfully for a number of mechanistic studies of enzyme reactions involving transition metals (see ref 22 for a recent review). Although mercury is not a transition metal in the strictest sense because its 5d-shell is completely filled and does not participate in bonding, and in MerB the substrate contains a metal rather than the enzyme, there are many similarities between MerB and transition-metal-containing enzymes. In general, errors of 3−5 kcal mol^{-1} are expected for hybrid DFT calculations of enzyme reactions involving transition metals,[23] but these errors are systematic, not random. Thus, there is often significant error cancellation, making it possible to distinguish between likely and unlikely reaction pathways.

As described above, several mechanistic variants have been proposed for MerB catalysis (see ref 14 for a concise summary of mechanistic hypotheses), but the X-ray structures help narrow the proposals to two main alternatives that we consider here (Figure 1): direct protonation of the carbanion leaving group by cysteine (Cys96 or Cys159) (Mechanism I), and abstraction of a proton from cysteine by Asp99, followed by protonation of the carbanion leaving group by Asp99 (Mechanism II). On the basis of X-ray structures of the Hg(II)-product-bound enzyme (Figure 2), we have constructed quantum chemical models of the active site of MerB with the methylmercury ($[CH_3Hg(II)]^+$) substrate. We employ a hybrid DFT method to describe the structures and energetics of intermediates and transition states corresponding to these two proposed mechanisms for the Hg−C protonolysis reaction catalyzed by MerB.

(8) Pitts, K. E.; Summers, A. O. *Biochemistry* **2002**, *42*, 10287–10296.
(9) Lafrance-Vanasse, J.; Lefebvre, M.; Lello, P. D.; Sygusch, J.; Omichinski, J. *J. Biol. Chem.* **2008**, *284*, 938–944.
(10) Momany, C.; Summers, A.; Cagle, C.; Teske, J. PDB ID 3FN8. Unpublished data.
(11) Gopinath, E.; Bruice, T. *J. Am. Chem. Soc.* **1987**, *109*, 7903–7905.
(12) Wilhelm, M.; Deeken, S.; Berssen, E.; Saak, W.; Lutzen, A.; Koch, R.; Strasdeit, H. *Eur. J. Inorg. Chem.* **2004**, 2301–2312.
(13) Ni, B.; Kramer, J. R.; Bell, R. A.; Werstiuk, N. H. *J. Phys. Chem. A* **2006**, *110*, 9451–9458.
(14) Miller, S. M. *Nat. Chem. Biol.* **2007**, *3*, 537–538.
(15) Barone, V.; Bencini, A.; Totti, F.; Uytterhoeven, M. *Organometallics* **1996**, *15*, 1465–1469.
(16) Barone, V.; Bencini, A.; Totti, F.; Uytterhoeven, M. *Int. J. Quantum Chem.* **1997**, *61*, 361–367.
(17) Warshel, A.; Levitt, M. *J. Mol. Biol.* **1976**, *103*, 227–249.
(18) Senn, H. M.; Thiel, W. *Curr. Opin. Chem. Biol.* **2007**, *11*, 182–187.
(19) Senn, H. M.; Thiel, W. *Top. Curr. Chem.* **2007**, *268*, 173–290.
(20) Himo, F. *Theor. Chem. Acc.* **2006**, *116*, 232–240.
(21) Siegbahn, P. E. M.; Himo, F. *J. Biol. Inorg. Chem.* **2009**, *14*, 643–651.
(22) Siegbahn, P. E. M. *J. Biol. Inorg. Chem.* **2006**, *11*, 695–701.
(23) Siegbahn, P. E. M.; Borowski, T. *Acc. Chem. Res.* **2006**, *39*, 729–738.

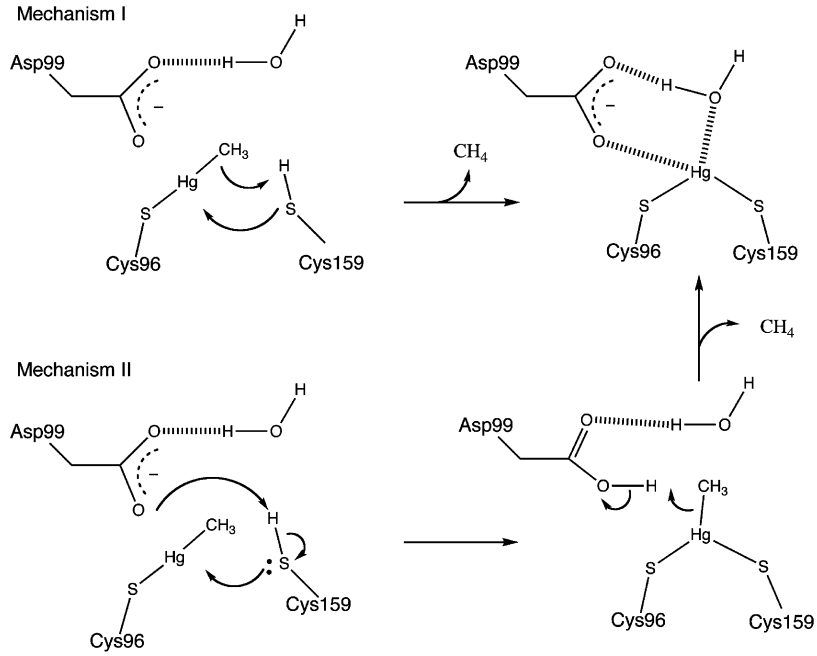

Figure 1. Proposed mechanisms for the Hg−C protonolysis reaction catalyzed by MerB. Both mechanisms assume that the methylmercury substrate has formed an initial covalent adduct with Cys96 and that Cys159 is initially protonated. In Mechanism I, Cys159 protonates the leaving group carbon as it coordinates with Hg(II). In Mechanism II, Cys159 donates a proton to Asp99 before coordinating with Hg(II). Asp99 then protonates the leaving group carbanion.

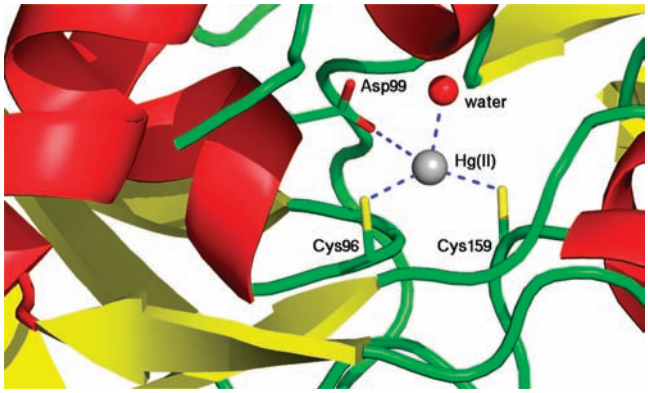

Figure 2. Active site of MerB from PDB ID 3F2F. Hg(II) and its ligands, Cys96, Asp99, Cys159 and a water molecule, are labeled.

We consider Cys96 and Cys159 as forming alternative initial covalent adducts with the substrate, and we also examine the reaction mechanism using two other known substrates, vinylmercury and *cis*-2-butenyl-2-mercury. We find that charge distributions in transition state structures can explain how MerB catalyzes the Hg−C protonolysis reaction, quantifying the roles of Cys96 and Cys159 in activating the Hg−C bond and of Asp99 in protonating the nascent carbanion leaving group.

Methods

We initially constructed quantum chemical models of the active site of MerB using an unpublished X-ray crystal structure of the Hg(II)-product-bound enzyme[10] as a template and refined them with the recently published structure.[9] Included in the model are the side chains of Cys96, Asp99, and Cys159, the product Hg(II), and the water molecule that appears in all X-ray crystal structures (Figure 2). Cys160 was not included in the model because it is not essential for activity.[8] A methane molecule (or ethylene or *cis*-2-butene), corresponding to the hydrocarbon protonolysis product of the reaction, was placed manually near the active site. The C_α atoms of Cys96, Asp99, and Cys159 were modeled as methyl groups and were constrained to their crystallographic positions. The entire system consisted of 35 atoms. For the reaction pathways considered (Mechanisms I and II, Figure 1), we assumed the substrate had already formed an initial covalent adduct with either Cys159 or Cys96 in the reactant state (see below). We considered the reaction only up to the formation of the Hg(II)-bound product complex observed in the X-ray experiments.

All electronic structure calculations were performed with the program Gaussian 03[24] using NSF TeraGrid resources.[25] The B3PW91 exchange-correlation functional[26,27] has been shown to provide a useful description of Hg and S chemistry[13,28] and was used throughout. Convergence criteria for self-consistent field and geometry optimizations were set to "tight" as defined in Gaussian 03.

For the geometry optimizations of the stationary point structures, we used the MWB60 (also called SDD) effective core potential (ECP) and basis set[29] for Hg and the 6-31G(d) basis set for all other atoms. Transition states were obtained using the quadratic synchronous transit method[30,31] (QST3) implemented in Gaussian 03 and were in each case verified using WebMO[32] by the presence of a single imaginary vibrational frequency associated with the desired reaction coordinate. The effects of the surrounding protein environment and solvent were modeled using the C-PCM

(24) Frisch, M. J. et al. *Gaussian 03, Revision E.01*; Gaussian, Inc.: Wallingford, CT, 2004.
(25) Catlett, C. TeraGrid: Analysis of Organization, System Architecture, and Middleware Enabling New Types of Applications. *High Performance Computing (HPC) and Grids in Action*; IOS Press: Amsterdam, 2007; Vol. 16 of Advances in Parallel Computing. .
(26) Becke, A. D. *J. Chem. Phys.* **1993**, *98*, 5648–5652.
(27) Perdew, J. P.; Wang, Y. *Phys. Rev. B* **1992**, *45*, 13244–13249.
(28) Tai, H. C.; Lim, C. *J. Phys. Chem. A* **2006**, *110*, 452–462.
(29) Andrae, D.; Haeussermann, U.; Dolg, M.; Stoll, H.; Preuss, H. *Theor. Chem. Acc.* **1990**, *77*, 123–141.
(30) Peng, C.; Schlegel, H. B. *Isr. J. Chem.* **1993**, *33*, 449–454.
(31) Peng, C.; Ayala, P. Y.; Schlegel, H. B.; Frisch, M. J. *J. Comput. Chem.* **1996**, *17*, 49–56.
(32) Schmidt, J. R.; Polik, W. F. *WebMO Pro*; WebMO, LLC: Holland, MI. Available from http://www.webmo.net.

Table 1. Comparison of Selected Geometric Parameters[a] in Crystal Structures and the DFT Model of the Hg(II)-Bound MerB Product Complex

	PDB ID				
	3F0P	3F2F	3F2H	3FN8	DFT[b]
Hg−S(Cys96)	2.3/2.3	2.4/2.4	2.5/2.4	2.4/2.3	2.44
Hg−S(Cys159)	2.4/2.4	2.5/2.5	2.5/2.5	2.3/2.1	2.46
Hg−O(Asp99)	2.9/3.2	2.9/3.0	3.1/3.1	2.9/2.9	2.46
Hg−O(water)	2.6/2.6	2.5/2.6	2.6/2.7	2.5/−	2.54
S(Cys96)−O(Asp99)	3.7/3.8	3.8/3.7	3.8/3.7	3.7/3.8	3.82
S(Cys159)−O(Asp99)	4.4/4.6	4.4/4.4	4.6/4.8	4.4/4.2	3.82
S(Cys96)−Hg−S(Cys159) angle	126/131	119/128	127/129	137/134	148.4

[a] Distances (Å) and angles (deg) are shown for both chain A and chain B in the crystallographic dimers. [b] DFT Model A. Initial coordinates were taken from the X-ray structure of Hg(II)-bound MerB (PDB ID 3F2F).

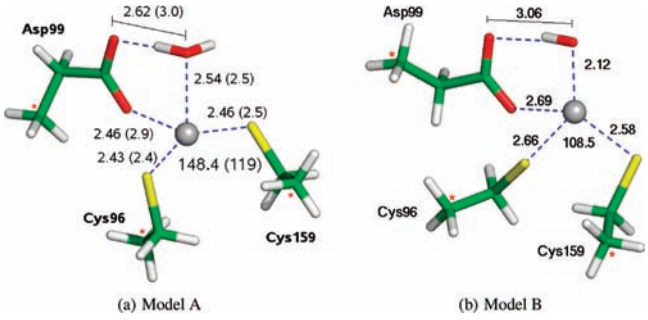

Figure 3. DFT optimized structures of the product states for (a) Model A and (b) Model B. In both cases, the C_α atoms of Cys96, Asp99, and Cys159 (denoted by red stars) were constrained to their crystallographic positions. Calculated bond distances (Å) and angles (deg) are labeled, with crystallographic values from PDB ID 3F2F in parentheses.

method[33−36] with a dielectric constant of 4.0. Single-point energies were computed at the optimized geometries using the SDD basis set and ECP for Hg and the 6-311++G(3df,2p) basis set for all other atoms. Natural Population Analysis (NPA)[37,38] was used to compute atomic partial charges and determine the orbital occupancies in a set of compact, localized orbitals. The NBO Version 3.1 program[39] implemented in Gaussian 03 was used to perform NPA.

Results

Structural Validation of the Active Site Model. In the crystal structure of the Hg(II)-bound product complex, the oxygen atom of a water molecule or hydroxide ion appears important in stabilizing the trigonal coordination geometry (Figure 2). Although the Hg−O distances observed crystallographically (Table 1) suggest that the oxygen atom belongs to a water molecule rather than a hydroxide ion, both cases were tested by performing geometry optimizations of two active site models (Figure 3) in which the oxygen was modeled as part of a water molecule (Model A) or a hydroxide ion (Model B). These optimizations served two purposes: first, to confirm the protonation state of the active site water molecule and, second, to assess the validity of the chosen quantum chemical method and the truncated active site model by comparing the computed structures with the X-ray data.

The optimized Model A reproduces the crystallographic structures more accurately (Figure 3), having a Hg−O(water) distance of 2.58 Å, well within the range of 2.5−2.7 Å observed in the various Hg(II)-bound crystal structures of MerB (Table 1). In contrast, the Hg−O(hydroxide) distance in Model B is 2.12 Å, significantly shorter than the experimentally observed distances. Similarly, the Hg−S distances are 2.44 and 2.45 Å for Model A, in agreement with the crystallographic range of 2.3−2.5 Å (Table 1), but for Model B they are 2.66 and 2.58 Å, significantly longer than the experimentally observed distance. For Model A, the optimized S−Hg−S angle is 149.3°, somewhat larger than the crystallographic range of 119−137°. For Model B, the S−Hg−S angle is 108.5°.

As an additional test of the geometric accuracy of the two models, we manually constructed reactant states corresponding to the product structures for Models A and B with methylmercury serving as the substrate. We assumed that the substrate had formed a covalent adduct with Cys159, as previously suggested.[8] In both cases Cys96 was protonated and Asp99 was deprotonated, as would be expected at physiological pH if the pK_a's were not perturbed by the active site environment. The electrostatic repulsion imparted by the additional negative charge from the hydroxide caused the Model B structure to rearrange to form a linear HO−Hg−CH_3 loosely coordinated to the Cys159 thiolate, and Cys96 spontaneously transferred its proton to Asp99 (not shown). In contrast, the reactant for Model A maintained a coordinated geometry similar to the product structure, suggesting that Model A represents the relevant protonation states for all participants at the outset of the reaction; thus, these were used for all further studies.

Characterization of Stationary Points. Optimizations of each stationary point with the methylmercury substrate were performed as described above for Model A, and reaction pathways were computed for Mechanisms I and II (Figure 1), beginning with methylmercury bound to either (a) Cys159 or (b) Cys96 for a total of four pathways (Figure 7). For Mechanism I, the pathway beginning with a methylmercury-Cys159 adduct is preferred energetically and is referred to as Mechanism I-a. For Mechanism II, the activation barriers for the reactions involving initial methylmercury adduct formation with Cys159 (Mechanism II-a) and Cys96 (Mechanism II-b) are quite similar energetically. Although the transition state (TS-2) is the same in both cases, lower energy intermediates were obtained for Mechanism II-b (Figure 7). In all pathways, the product state (PS-1) is identical, and each process is consistent with an S_E2 mechanism. Stationary point structures for all pathways are provided as Supporting Information.

Mechanism I-a. In Mechanism I-a, the reaction process consists of a single step (Figure 4) beginning with RS-2, which is characterized by a Hg−S(Cys159) bond of 2.43 Å and a protonated Cys96 hydrogen bonded to Asp99. As S(Cys96) approaches R−Hg(II) at the transition state (TS-4), the thiol proton (H-1) is transferred to the leaving group carbon (C_{LG}) in concert with Hg−C cleavage. The experimental turnover number (k_{cat}) for MerB with CH_3HgCl is 0.7 min^{-1},[7] corresponding to an activation free energy of 20.1 kcal mol^{-1} at 298 K (Table 2) as calculated using transition-state theory. In contrast, the calculated activation energy for Mechanism I-a is 33.9 kcal mol^{-1} (Figure 7), significantly higher than the experimental value. The distance between S(Cys96) and Hg in

(33) Klamt, A.; Schüürmann, G. *J. Chem. Soc., Perkins Trans.* **1993**, *2*, 799–805.
(34) Andzelm, J.; Kölmel, C.; Klamt, A. *J. Chem. Phys.* **1995**, *103*, 9312–9320.
(35) Barone, V.; Cossi, M. *J. Phys. Chem. A* **1998**, *102*, 1995–2001.
(36) Cossi, M.; Rega, N.; Scalmani, G.; Barone, V. *J. Comput. Chem.* **2003**, *24*, 669–681.
(37) Reed, A.; Weinstock, R. B.; Weinhold, F. *J. Chem. Phys.* **1985**, *83*, 735–746.
(38) Reed, A.; Curtiss, L.; Weinhold, F. *Chem. Rev.* **1988**, *88*, 899–926.
(39) Glendening, E. D.; Reed, A. E.; Carpenter, J. E.; Weinhold, F. *NBO Version 3.1*.

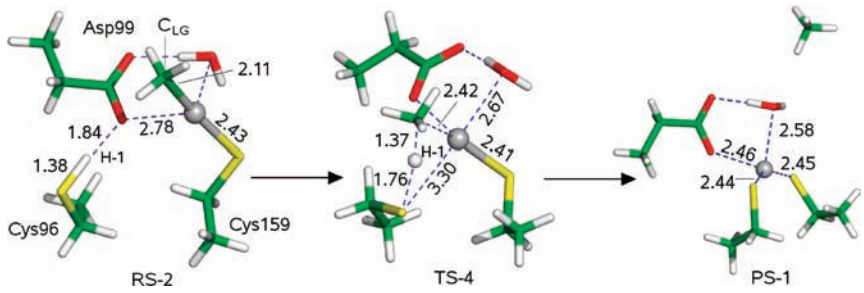

Figure 4. DFT-optimized stationary point structures for Mechanism I-a in which the substrate has formed an initial covalent adduct with Cys159. Important distances (Å) are labeled. Colors: Hg, silver; C, green; S, yellow, O, red; H, white.

Table 2. Experimental and Calculated Activation Barriers for Organomercurial Substrates[a]

substrate	turnover no.[b] (min^{-1})	$\Delta G^{\ddagger}_{298K}$	$\Delta E^{\ddagger}_{Mech\ II\text{-}a}$	$\Delta E^{\ddagger}_{Mech\ II\text{-}b}$
$[CH_3Hg(II)]^+$	0.7	20.1	20.4	22.4
$[CH_2{=}CH{-}Hg(II)]^+$	12	18.4	18.3	18.4
[*cis*-2-butenyl-2-Hg(II)]$^+$	240	16.6	15.6	16.4

[a] All energies in kcal mol^{-1}. [b] Data from ref 7.

TS-4 is quite long at 3.30 Å but resembles the geometries of other computed transition state structures involving direct protonolysis by model compound thiols, which are characterized by incomplete coordination between Hg and the thiol proton donor, Hg−C bond elongation, and linear proton transfer between the thiol and C_{LG}.[12,13] As the Hg−C bond lengthens from 2.11 Å in RS-2 to 2.42 Å in TS-4, the Hg−O(Asp99) distance decreases from 2.78 to 2.38 Å. Asp99 partially compensates for weak Hg−S(Cys96) coordination in TS-4 by interacting with Hg. However, a carboxylate is not as strong an activator of the Hg−C bond as is a thiolate,[28] consistent with the high activation energy of Mechanism I-a.

Mechanism I-b. In Mechanism I-b, the reaction begins with RS-2 and proceeds via TS-5 (Supporting Information) to form PS-1. Because the activation barrier for Mechanism I-b (36.0 kcal mol^{-1}, Figure 7) is quite similar but even higher than that for Mechanism I-a, Mechanism I-b is not discussed further.

Mechanism II-a. Mechanism II-a involves two chemical steps (Figure 5). In the first step, H-1 is transferred from Cys96 to Asp99 with a nearly barrierless transition state (TS-3) to form INT-4. Upon geometric rearrangement, Cys96 coordinates with R−Hg(II) in the second chemical step and Asp99 protonates C_{LG} at the transition state (TS-2) to release methane and form the Hg(II)-bound product structure. Participation of Asp99 in a proton relay significantly lowers the activation energy compared to that of Mechanism I-a because it enables complete Hg−S coordination by both Cys96 and Cys159 at the transition state (TS-2). As RS-2 is predicted to be slightly lower in energy than INT-4, the activation barrier for Mechanism II-a is the difference in energy between TS-2 and RS-2, which is 20.4 kcal mol^{-1} (Figure 7), in close agreement with the experimental activation free energy of 20.1 kcal mol^{-1}.[7]

Mechanism II-b. Mechanism II-b involves two chemical steps and several geometric rearrangements (Figure 6). RS-1 is characterized by a covalent Hg−S(Cys96) bond length of 2.40 Å, a hydrogen bond between Cys159 and Asp99, and the water molecule centrally located between Hg, Asp99, and Cys159. RS-1 rearranges to form INT-1, in which the water molecule bridges between Cys159 and Asp99. In the first chemical step, Cys159 donates a proton to Asp99 in a concerted, water-assisted process (TS-1) to form INT-2, which then rearranges to form the energetically more favorable INT-3.

In the second chemical step, deprotonated Cys159 provides a second thiolate ligand for R−Hg(II) at the transition state (TS-2), and Asp99 protonates C_{LG} to liberate methane and form the Hg(II)-bound product (PS-1). As INT-3 is predicted to be the

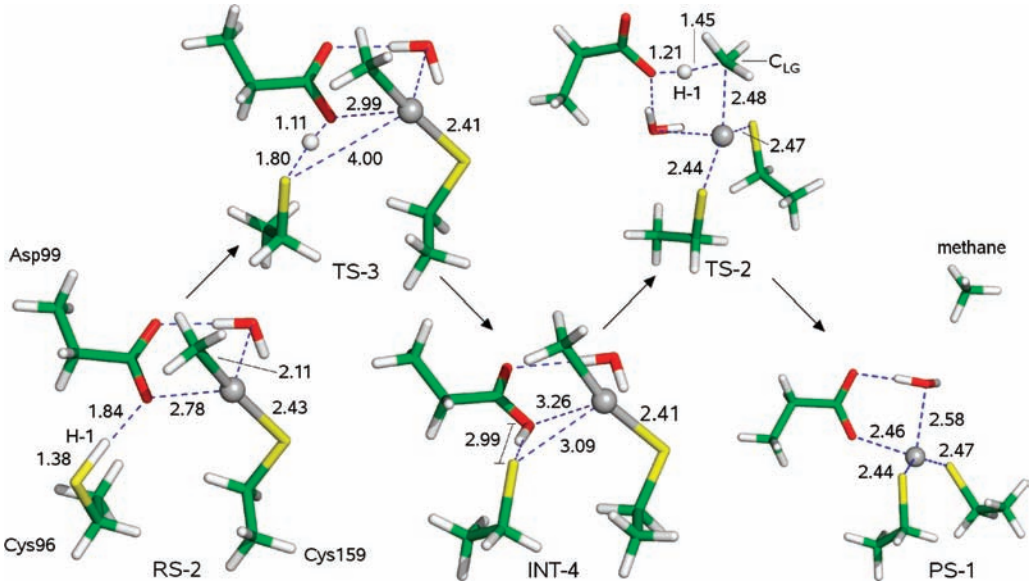

Figure 5. DFT-optimized stationary point structures for Mechanism II-a in which the substrate has formed an initial covalent adduct with Cys159. Important distances (Å) are labeled. Colors: Hg, silver; C, green; S, yellow, O, red; H, white.

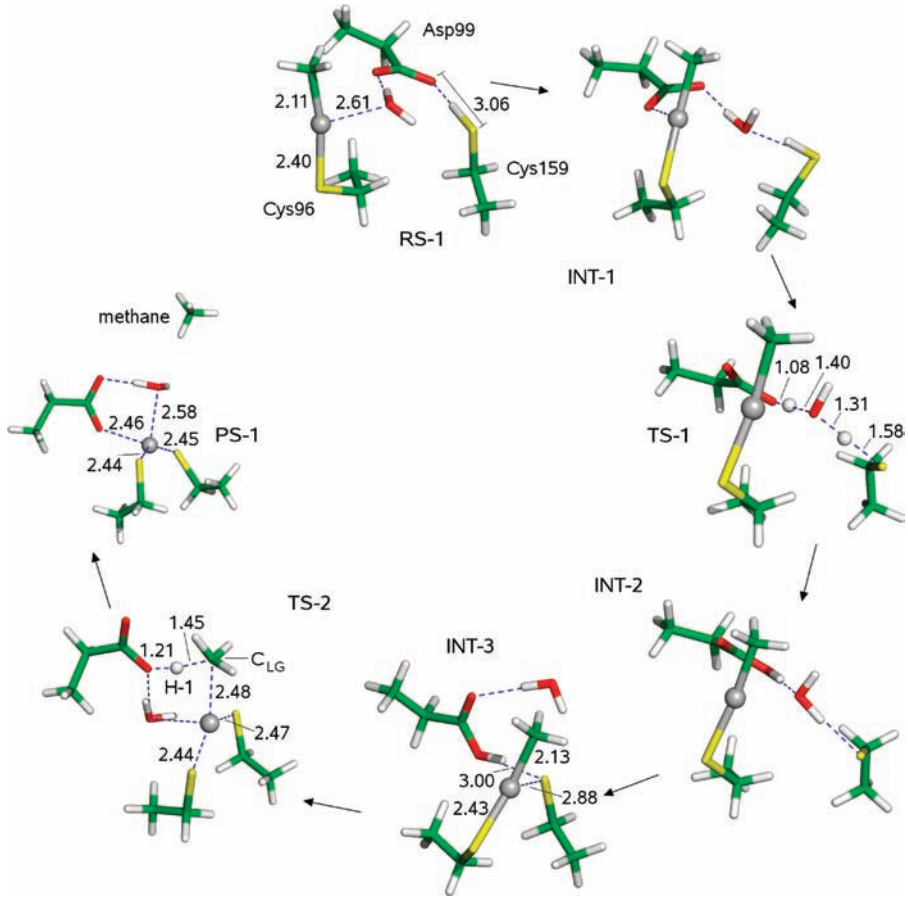

Figure 6. DFT-optimized stationary point structures for Mechanism II-b in which the substrate has formed an initial covalent adduct with Cys96. Important distances (Å) are labeled. Colors: Hg, silver; C, green; S, yellow, O, red; H, white.

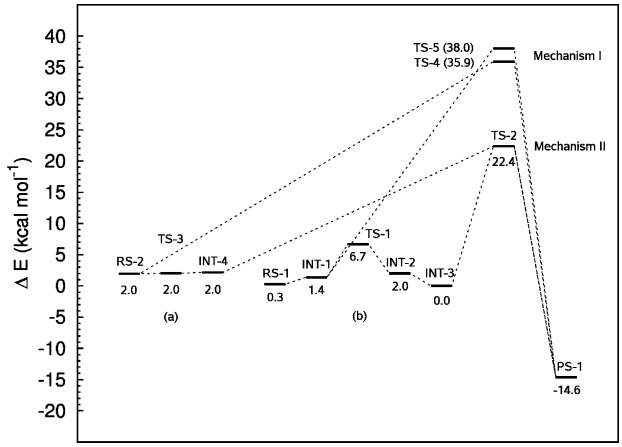

Figure 7. DFT total energy profiles for Mechanisms I and II beginning from initial methylmercury adducts with (a) Cys159 and (b) Cys96. All energies are in kcal mol^{-1} relative to INT-3.

lowest in energy of all reactants and intermediates for Mechanism II-b, the activation energy for methylmercury protonolysis is the difference in energy between TS-2 and INT-3, which is 22.4 kcal mol^{-1} (Figure 7), also in good agreement with experiment. As in Mechanism II-a, the Asp99-mediated proton relay significantly lowers the activation energy compared to that of Mechanism I-a ($\Delta\Delta E^{\ddagger} = -11.5$ kcal mol^{-1}). Consistent with this idea, the Hg−C bond in TS-2 (2.48 Å) is slightly longer than in TS-4 (2.42 Å), suggesting that the bond is weaker in TS-2 and therefore more susceptible to cleavage.

To examine the influence of the proposed proton relay on the eventual ligation of the second cysteine thiolate ligand to Hg, we examined Hg−S bonding in the absence of competing interactions from Asp99. For this calculation, the C_α atoms of Cys96 and Cys159 were constrained as Figure 3, but Asp99 and the water molecule were deleted. Geometry optimization of this complex yields a trigonal planar structure with symmetric Hg−S bond lengths of 2.56 Å and a Hg−C bond length of 2.18 Å (Figure S2, Supporting Information). Thus, hydrogen bonding between Asp99 and Cys96 in INT-4 (Figure 5) or between Asp99 and Cys159 in INT-3 (Figure 6) can hinder formation of the second Hg−S bond. This result suggests that proton transfer to Asp99 from cysteine in the first step of the reaction must be completed to enable bis thiol ligation and allow Asp99 to move into position for protonation of the leaving group.

Role of Water. To investigate the role of the water molecule coordinated to Hg(II) in the X-ray crystal structures, we computed reaction paths for Mechanisms I and II in which the explicit water molecule was deleted. The water molecule was found to have only a nominal stabilizing effect on the transition state, lowering the activation barrier for Mechanism II by 1.2 kcal mol^{-1}, with a similar but greater stabilization (2.5 kcal mol^{-1}) for Mechanism I (Figure S1, Supporting Information).

Natural Population Analysis. The analysis of charge displacements can provide useful insight into the mechanism of transition state stabilization. Here, we employ NPA, which provides an intuitive, localized representation of the electron density associated with each atom in a molecular system.[37,38] NPA involves transforming the molecular orbitals into orthonormal,

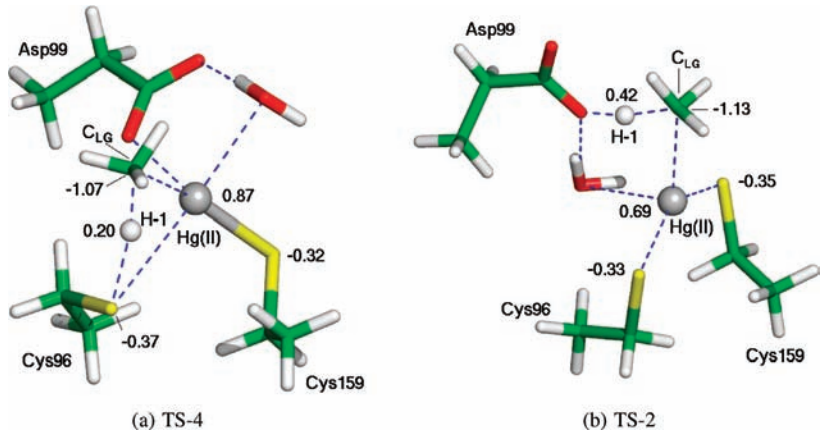

Figure 8. NPA atomic partial charges for selected atoms in (a) TS-4 and (b) TS-2.

"natural" atomic orbitals. The NPA partial atomic charges are simply the sum of the resulting electronic occupancies and the nuclear charge on a given atomic center.

NPA was performed on TS-2 and TS-4, revealing key differences in the electron distributions between the highest-energy transition states for Mechanism I-a (TS-4) and Mechanism II-a/b (TS-2) (Figure 8). Mercury in the substrate R−Hg(II) has a formal charge of +2, but there is significant charge transfer from the thiolate ligand(s) in the activated complex, as Hg has an NPA partial atomic charge of +0.87 in TS-4 and +0.69 in TS-2. In TS-2, Hg is covalently bound to both S(Cys159) and S(Cys96), resulting in an increased occupancy of the 6s and 6p orbitals of Hg relative to TS-4, in which Cys159 is covalent bound to Hg but Cys96 is only weakly coordinated. The charge on C_{LG} is slightly more negative (by 0.06) in TS-2 than TS-4, indicating that the leaving group is more susceptible to attack by an electrophilic proton when the substrate is coordinated to both thiolates (Cys96 and Cys159).

The most pronounced difference between the two transition states is in the charge on the catalytic proton H-1 (Figure 8). In TS-4, the charge on H-1 is +0.20, indicating that it retains a significant amount of electron density from S(Cys96) in Mechanism I-a. In TS-2, however, the charge on H-1 is +0.42, indicating stronger electrophilic character relative to H-1 in TS-4. Thus, the combined slight increase in C_{LG} electronegativity and the considerable increase in H-1 electrophilicity in TS-2 versus TS-4 favor Hg−C protonolysis in Mechanism II-b.

Other Substrates. Among organomercurials that undergo protonolysis by MerB, methylmercury chloride has the slowest observed reaction rate.[7] Additional tests of Mechanisms II-a and II-b were performed for vinylmercury and *cis*-2-butenyl-2-mercuryl; the latter is a "fast" organomercurial substrate (turnover number of 240 min^{-1}) and the former is intermediate (12 min^{-1}) between the two limiting cases. The substrates were positioned manually in the active site, and the reactions were modeled in an analogous way to the methylmercury reaction. The computed activation barriers (Table 2) reproduce the trend in experimental activation free energies. For methylmercury, the computed barriers are 20.4 kcal mol^{-1} for Mechanism II-a and 22.4 kcal mol^{-1} for Mechanism II-b, comparing favorably to the experimental activation free energy of 20.1 kcal mol^{-1}. For vinylmercury and *cis*-2-butenyl-2-mercury, the computed barriers for Mechanisms II-a and II-b are essentially identical to the experimental activation free energies. The agreement with experiment indicates that the continuum representation of the surrounding enzyme and solvent environment accurately describes environmental effects on the MerB protonolysis reaction. Therefore, being within 1 kcal mol^{-1} of experiment on average, the active site DFT model captures the essence of the MerB reaction mechanism and provides quantitative support for the thiol-base-acid relay as the energetically favored mechanism.

Discussion

Transition State Stabilization. Both Mechanism I and Mechanism II agree with work on synthetic models of MerB that has demonstrated the importance of multiple Hg−S coordination for Hg−C protonolysis reactions.[3] A key feature of Mechanism II-a is the large decrease in the distance between R−Hg(II) and S(Cys96) from 3.09 to 2.44 Å in going from INT-4 to TS-2 (Figure 5). Similarly, in Mechanism II-b the distance between R−Hg(II) and S(Cys159) decreases from 2.88 to 2.47 Å in going from INT-3 to TS-2 (Figure 6), indicating that transition-state stabilization in Mechanisms II-a and II-b depends in part on the enhancement in the binding energy imparted by complexation of R−Hg(II) with the second thiolate ligand at the transition state; the function of any catalyst depends on its affinity for the altered substrate in the transition state.[40]

The driving force for deprotonation of S(Cys96) in Mechanism II-a, or S(Cys159) in Mechanism II-b, may be the affinity of R−Hg(II) for an additional thiolate ligand, since an aspartic acid would not be expected to abstract a proton from a cysteine. However, the Hg−S(Cys96) distance in INT-4 is 3.09 Å (Figure 5), and complete Hg−S(Cys96) ligation does not occur until TS-2 is formed. The formation of the Hg−S(Cys96) bond in INT-4 is delayed because, based on the O(Asp99)−S(Cys159) distance of 2.99 Å, the Cys96 thiolate is transiently hydrogen bonded with aspartic acid.

Initial Cysteine Nucleophile. Cys96 lies at the N-terminus of an α-helix, and such an arrangement of helix dipoles can lower cysteine pK_a values significantly.[41] Depending on the extent to which the Cys96 pK_a is lowered, there are two possible consequences. A large shift in pK_a would mean that Cys96 is always a thiolate and thus would readily attack the substrate to form the initial enzyme−substrate adduct, followed by Cys159 providing the catalytic proton to Asp99, either directly or via an intermediary water molecule (as in Mechanism II-b). A less drastic pK_a shift could result in Cys96 being protonated prior to substrate binding, but with a pK_a closer to that of Asp99,

(40) Wolfenden, R.; Kati, W. M. *Acc. Chem. Res.* **1991**, *24*, 209–215.
(41) Kortemme, T.; Creighton, T. *J. Mol. Biol.* **1995**, *253*, 799–812.

making the proton transfer from Cys96 to Asp99 more favorable (as in Mechanism II-a).

It has been proposed previously that the organomercurial substrate is attacked first by either Cys159[8] or Cys96.[9] Mechanisms II-a and II-b are closely similar mechanistically and energetically. In comparing the energy profiles for Mechanisms II-a and II-b (Figure 7), the lower energies of the reactant and intermediate states in Mechanism II-b relative to those in Mechanism II-a may actually confer a catalytic disadvantage because they result in a net increase in the activation barrier. Thus, the slightly higher energy enzyme−substrate complex in Mechanism II-a may be a means of reducing the activation barrier in the Hg−C protonolysis reaction. However, the small differences in energies between Mechanisms II-a and II-b are within the uncertainty of the method. Consequently, the possibility that either cysteine attacks the organomercurial substrate remains. In both cases, the Asp99-mediated proton relay mechanism of transition state stabilization for the Hg−C protonolysis step would be the same.

Given that it is equally likely that Cys159, rather than Cys96, forms the initial covalent adduct with the substrate, it is noteworthy that Cys96 is the closer of the two cysteines to Asp99 (3.8 versus 4.4 Å, Table 1) and is therefore more likely to donate a proton directly to Asp99. Although we have shown that a water molecule may facilitate proton transfer from Cys159 to Asp99 (Figure 6), a simpler pathway involves direct proton transfer from Cys96 to Asp99 (Figure 5). Moreover, Cys96 is located at the N-terminus of an α-helix, which may lower its pK_a (see above), making proton transfer from Cys96 to Asp99 more facile.

Mechanistic Implications. The present QM modeling has enabled a quantitative description of a thiol−base−acid proton relay mechanism for Hg−C cleavage by MerB. The present work confirms that Asp99 is the proton donor, as suggested previously.[9] Furthermore, a mechanism of transition state stabilization is revealed. The calculations show that the bulk of the catalytic chemistry of MerB comes from only three groups, Cys96, Cys159, and Asp99. At the rate-limiting transition state, coordination of R−Hg(II) by two cysteines induces redistribution of electron density into Hg(II) and C_{LG} and away from the catalytic proton on Asp99.

Conclusions

In the present work, quantum chemical calculations have been performed to compare the two chief candidate mechanisms for the Hg−C protonolysis catalyzed by the organomercurial lyase, MerB. Using an active site cluster model generated from the Hg(II)-product-bound X-ray crystal structure of MerB, an Asp99-mediated proton relay mechanism has been determined for MerB. The calculations suggest that formation of the initial methylmercury adduct either by Cys96 or Cys159 is energetically feasible. Our results establish quantitatively that coordination of R−Hg(II) by two cysteine thiolates is necessary and sufficient to activate the Hg−C bond toward protonolysis. Moreover, we have shown that bis coordination of R−Hg(II) induces redistribution of electron density into Hg(II) and the leaving group carbon and away from the catalytic proton on Asp99.

In the present work, we have computationally dissected a critical aspect of the mechanism of bacterial mercury resistance, the MerB-catalyzed demethylation of organomercurials. This information contributes fundamental understanding of biological systems involved in the transformation of mercury species in the environment. It provides a basis for developing strategies to lower methylmercury levels in contaminated ecosystems, where past mercury use has resulted in methylmercury accumulation in biota.

Acknowledgment. This research was sponsored by the U.S. Department of Energy Office of Science, Biological and Environmental Research, Environmental Remediation Sciences Program (ERSP). Oak Ridge National Laboratory is managed by UT-Battelle, LLC, for the U.S. Department of Energy under contract DE-AC05-00OR22725. Computer time was provided by the National Science Foundation through TeraGrid resources provided by NCSA (Grants TG-MCA08X032 and TG-CHE090017). We thank Hao-Bo Guo and Alexander Johs for helpful discussions and an anonymous reviewer for providing many useful comments.

Supporting Information Available: Optimized coordinates and energies for all stationary point structures, NPA charges for TS-4 and TS-2, and complete ref 24. This material is available free of charge via the Internet at http://pubs.acs.org.

JA9016123